

Melting of Gold Clusters: Icosahedral Precursors

Charles L. Cleveland, W. D. Luedtke, and Uzi Landman

*School of Physics, Georgia Institute of Technology,
Atlanta, Georgia 30332-0430*

(Received 2 March 1998)

Investigations of the melting of gold nanocrystalline clusters, using molecular dynamics simulations, reveal that at elevated temperatures the melting process is punctuated by solid-to-solid structural transformations from the low-temperature optimal structures (a truncated octahedron for Au₄₅₉, and a truncated decahedron for Au₁₄₆) to icosahedral structures, occurring as precursors to the melting transitions. These precursors are intrinsic to the thermodynamics of the clusters and are not the result of extrinsic effects, such as charging and electrostatic interactions. [S0031-9007(98)07047-1]

PACS numbers: 36.40.Ei

The decrease in the melting temperature of materials clusters (in particular, metals) with reduction of their size has been long expected and observed [1–14]. Additionally, for small clusters (of the order of tens to a few hundred atoms) the first-order (sharp) bulk melting transition is broadened (exhibiting a characteristic S-shaped loop in the transition region [11]). In almost all treatments, these phenomena are related to considerations involving interior (bulk) and surface regions of the cluster, with the surface acting as a source for premelting effects; that is, thermal activation of low-coordinated and weaker bonded surface atoms at edges and corners between surface facets [6,7], and formation of a surface wetting quasiliquid layer at $T < T_M$ (bulk), in analogy with the well studied premelting process of extended crystalline surfaces [15].

Furthermore, simulation studies of clusters have led to generalization of the (bulk) concept of equilibrium thermodynamic phase coexistence to include “dynamic coexistence” (DC) states [7(b)], occurring in relatively small clusters where in a temperature range in the vicinity of melting an individual cluster may fluctuate in time between being entirely solid or liquid. In the DC regime the issue of time scales is of importance, and results depend on the length of the observation time relative to the mean interval spent in the different phases and to the transit time between them. On the other hand, for larger clusters “conventional” equilibrium phase coexistence may be established (see Ref. [10] and references therein), as is the case in our study; that is, the equilibrium states of the cluster (in the transition region) consist at all times of coexisting solid and liquid fractions.

The melting scenario described here for gold nanoclusters differs from the aforementioned surface premelting one (see, e.g., Ref. [6]). We predict, through extensive molecular dynamics (MD) simulations of Au_n clusters, that as a precursor to melting these clusters undergo at elevated temperatures *solid-to-solid transformations* from the low-temperature optimal structural motifs [16] (truncated decahedra, Dh, for $n < 250$, and truncated octahedra, TO, for larger clusters) to an icosahedral, Ih, structure, with

eventual melting of the latter below the bulk melting temperature. These structural transformations and icosahedral precursor states, punctuating the phase transition process, are intrinsic to the thermodynamics of the clusters, rather than the result of extrinsic effects (e.g., charging and consequent electrostatic interactions [4]).

In our MD simulations we used the many-body embedded-atom potential (EAM). These potentials have been used in our previous investigations of Au nanoclusters, resulting in the prediction of a discrete family of energetically optimal structures (i.e., a “magic number” sequence), which has been confirmed experimentally [16]. In this study we focus on two clusters from that family, belonging (at low temperatures) to different structural motifs; Au₄₅₉ with a TO⁺ structure [16(b),16(c)], and Au₁₄₆ with a (Marks) truncated-decahedral structure [16(a)]; we note here that, at low temperatures, structures based on icosahedral packing are energetically noncompetitive for gold clusters in this size range [see, e.g., Fig. 1 in Ref. [16(c)]]. The cluster simulations were performed by starting at room temperature and then incrementing the energy (through scaling of the atomic velocities) in steps, and equilibrating the cluster after each increment for long periods ($\sim 3 \times 10^5 \Delta t$, where $\Delta t = 3 \times 10^{-15}$ s is the integration time step) at constant energy; that is, the (kinetic) temperature is determined from the calculated mean kinetic energy of the atoms. The quantities which we show (results for Au₄₅₉ are displayed) were obtained as time averages over $2.5 \times 10^5 \Delta t$ following equilibration (with even larger equilibration and averaging periods in the transition regions).

In Fig. 1 we display for several temperatures histograms of the following: (a) The number of atoms N plotted versus the distance from the center of mass (c.m.) of the Au₄₅₉ cluster; (b) the atomic diffusion D evaluated as the slope of $R^2(t)/6 = \langle [r_i(t) - r_i(0)]^2 \rangle / 6$, where r_i is the vector position of the i th atom from the c.m. and the angular brackets denote averaging over time origins and atoms; and (c) the signatures of a common neighbor analysis (CNA) [17] serving for structural characterization. Also included

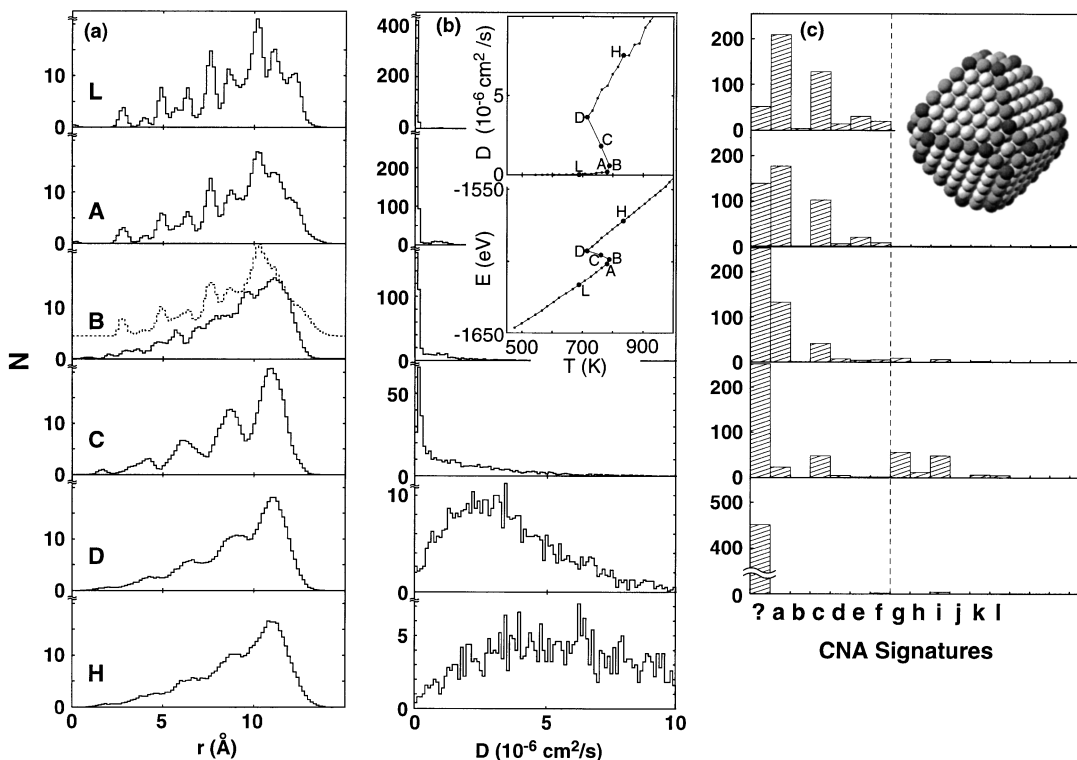


FIG. 1. Properties of an Au_{459} cluster at various states. (a) Radial atomic distributions, expressed as numbers of atoms (N) plotted versus distance from the center of mass of the cluster. In the panel marked B the light dotted curve (shifted upwards) corresponds to calculations with the atom closest to the center of mass as the origin. This distinction does not affect the other curves. (b) Corresponding histogram of the values of the atomic diffusion constant (in units of $10^{-6} \text{ cm}^2/\text{s}$). (c) Corresponding CNA signatures, denoted as follows: a : fcc (bulk); b : fcc (100) facet; c : fcc (111) facet; d : edge between (111) and (100) facets; e : (111)/(111) facets edge; f : fcc TO corner atom (vertex); g : icosahedral (Ih) internal twinning plane; h : Ih "spine" (atoms on the line connecting the center of an icosahedron to a surface vertex atom); i : (111)/(111) Ih edge; j : Ih central atom; k : Ih surface vertex; l : Ih surface vertex atoms created by removing an Ih vertex of type k ; "?" denotes noncrystallographic signatures, assigned to atoms which do not have any of the above ($a-l$) signatures. While both Ih and TO clusters have atomic signatures shown on the left of the dashed line, the signatures to the right of the dashed line are characteristic Ih ones. Inset of (b): caloric curve CC (total energy vs T) and the total diffusion in the cluster vs T . The points marked on the CC [and used to denote the respective rows of the figure, see upper case letters in column (a)] correspond to the following: L (688 K), A (782 K), B (788 K), C (760 K), D (715 K), and H (834 K). In the inset of (c) we show the TO equilibrium atomic configuration of Au_{459} . Distance and temperature in units of Å and Kelvin, respectively.

as an inset are the caloric curve, CC (i.e., the total energy of the cluster plotted vs T), and the total diffusion in the cluster vs T . From the CC we may estimate, following common practice (i.e., as the temperature at the midpoint of the "melting region," that is, between points B and D), an effective melting temperature $T_M \sim 760$ K, compared to T_M (bulk) = 1090 K calculated for the EAM gold material.

However, examinations of the structural and dynamic characteristics in Fig. 1, as well as inspection of Fig. 2, where cluster configuration/property plots are given, reveal the complex nature of the thermal evolution of the cluster. Following the development of the atomic radial distributions in Fig. 1(a) along the sequence of points marked on the caloric curve, it is observed that the well-formed atomic shells corresponding to crystalline order extending to the surface of the cluster for $T \leq 700$ K (see, e.g., point L), are gradually obliterated near the surface of the cluster as the temperature increases to $T \sim 788$ (point B). This sur-

face disordering process is portrayed by a decrease of the weights of CNA signatures [Figs. 1(c) and 2] corresponding to fcc-surface facets (coincident with the increase of noncrystallographic signatures), and in some "rounding" of the outer periphery of the cluster (see B in Fig. 2). At the same time, the scattering functions remain essentially unchanged (Fig. 3), and the overall mobility of atoms in the cluster remains low, with increased diffusion observed for surface edge and corner atoms [see the views corresponding to states A and B in Fig. 2, and Fig. 1(b)].

Unexpected dramatic structural and dynamic changes occur when the next state of the cluster is reached [point C in Fig. 1(b) (inset)], signaled by the reordering of the atomic radial distribution [compare B and C in Fig. 1(a)] and the appearance of icosahedral signatures in the CNA analysis [see fourth panel from the top in Fig. 1(c)]. Detailed analyses of the atomic trajectories and structural evolution indicate that this solid-to-solid transformation is essentially diffusionless, occurring rapidly and involving

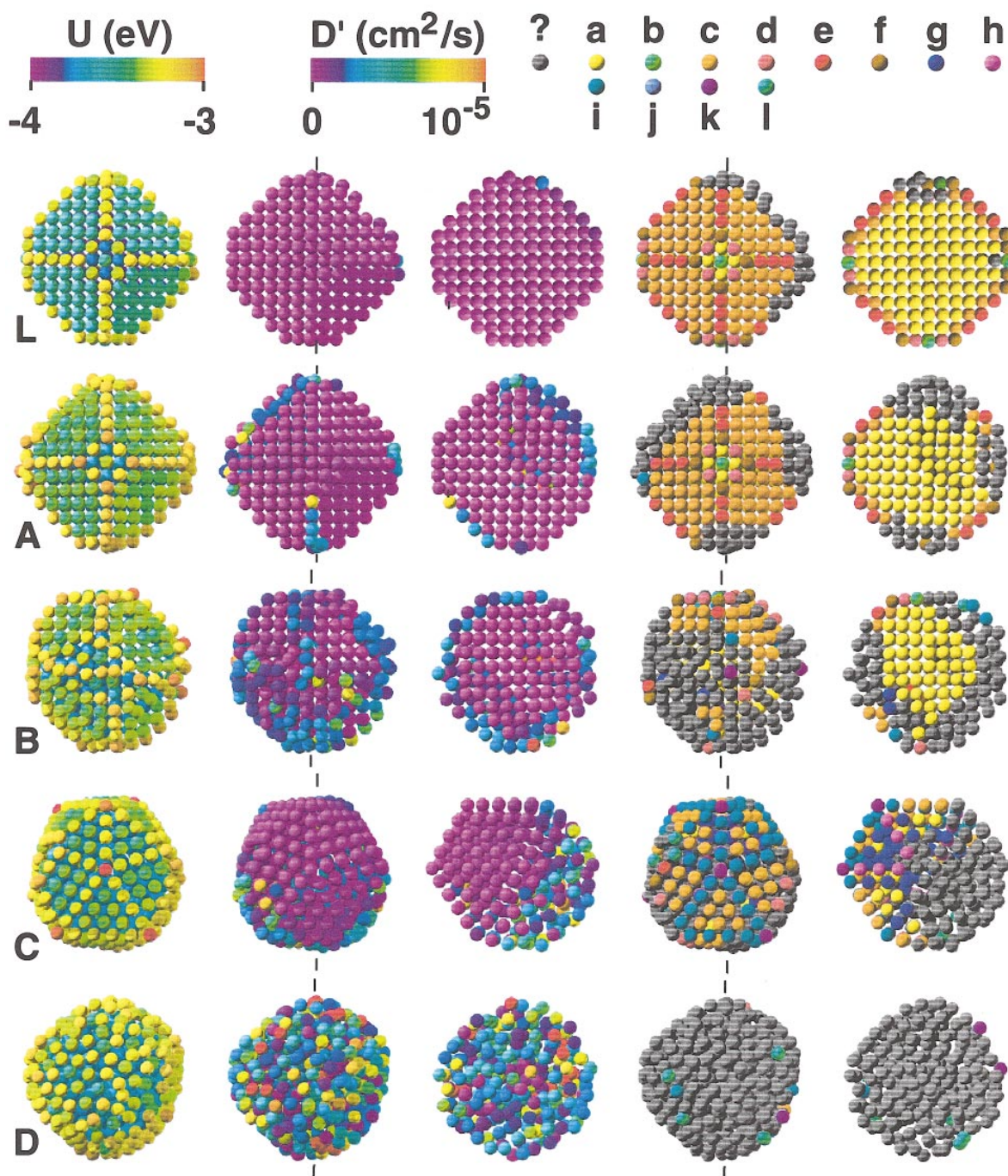


FIG. 2(color). Cluster configuration/property plots. The letters on the left correspond to those marked on the caloric curve [inset of Fig. 1(b)]. All the configurations (except the third and fifth columns) correspond to a view of Au_{459} along the normal to the front (100) facet of the cluster shown in the inset of Fig. 1(c). The columns of the figure correspond to the following: 1st column: potential energy U per atom (in eV); 2nd and 3rd columns: estimated atomic diffusion (calculated for each atom), in cm^2/s ; 4th and 5th columns: CNA characteristics. In the (2nd,3rd) and (4th,5th) columns the ones on the left (i.e., 2nd and 4th) correspond to views with the same cluster orientation as in the first column (U); the ones on the right (3rd and 5th) correspond to a view obtained via cutting the cluster in the middle with a meridian (north-south) plane normal to the page (the cut line is indicated in columns 2 and 4) followed by a 90° left rotation of the left half of the cluster (i.e., the plane of the cut lies in the plane of the page). The color codings and scales of U , D' , and the CNA signatures are given at the top.

a high degree of cooperative (small) displacements of the atoms; these characteristics are reminiscent of a martensitic transformation, though complicated by the finite size of the cluster. The structural transformation (driven by

the vibrational and configurational entropy of the cluster at elevated temperatures [19]) is most evident in the cluster configuration/property plots (see potential energy U and CNA signatures in Fig. 2 corresponding to C)

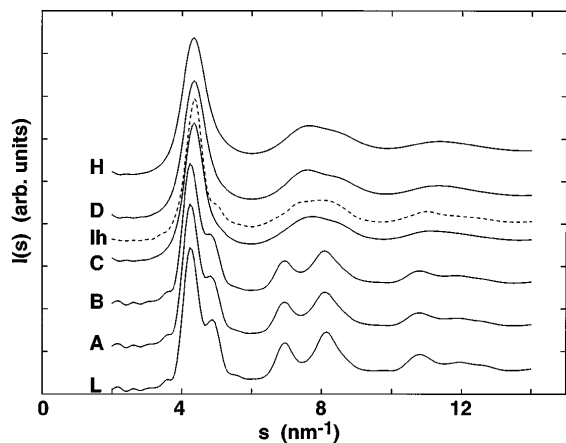


FIG. 3. Angle-averaged (powder) x-ray intensities, $I(s)$ (in arbitrary units) plotted vs the momentum transfer s (wave number in nm^{-1}), calculated, using the Debye formula [18] for the Au_{459} at the denoted states [corresponding to the points marked in the caloric curve, see inset of Fig. 1(b)]. The dashed line is the $I(s)$ calculated for an icosahedral Au_{561} cluster at $T = 740$ K. All the results were obtained via averaging $I(s)$ over 700 ps periods. s -dependent atomic gold scattering factors were used.

exhibiting formation of fivefold symmetry patterns, and it is reflected in the scattering function (compare B and C in Fig. 3). These changes are accompanied by an increased mobility in the cluster [see Fig. 2, and note the high-diffusion tail in Fig. 1(b) and the increase of the total diffusion coefficient (in the inset of Fig. 1(b))]. At this stage the cluster is at all times in a state of equilibrium coexistence between a solid (icosahedral) fraction and a liquidlike fraction exhibiting increased atomic mobility (see, in particular, the third column corresponding to C in Fig. 2), and appearing as a “pendant drop” rather than wetting around the icosahedral (solid) part (see columns 3 and 5 in Fig. 2). Reversal of the path on the caloric curve, i.e., $C \rightarrow B \rightarrow A$ starting from the above partial icosahedral configuration (C), results in recovery of the fcc structural motif (A).

True melting of the whole cluster occurs only at the next stage (marked D on the CC), with complete loss of crystalline signatures [Figs. 1(c) and 2], and a most significant increase in atomic diffusion [see Fig. 1(b), the inset, and Fig. 2]. We note here that the interior part of the liquified cluster maintains a loose shell structure [see D and H in Fig. 1(a)] and that the complete liquefaction does not alter in a significant manner the scattering function (compare C with D and H in Fig. 3).

The thermal evolution and melting scenario which we found for the smaller Au_{146} cluster also involved a structural transformation from a low-temperature equilibrium (truncated-decahedral) structure to an icosahedral one at ~ 500 K, with eventual melting occurring at ~ 650 K (i.e., a broader transition region than that for the Au_{459} cluster described above).

Structural instabilities and associated transformations were discussed previously for metal (gold) clusters (as

small as a few hundred atoms) in the context of high-resolution electron microscopy of supported particles [4,12], and have been attributed [4] to shearing forces acting on clusters adhered to surfaces, originating from (multiple) charging by the electron beam and consequent electrostatic interactions. In contrast, the structural-transformation (icosahedral) precursors to the melting transition of gold clusters, found in this study for neutral isolated clusters, are intrinsic thermodynamic states rather than the result of electronic excitations and other extrinsic effects, and they provide insights into the nature of phase transformations of metal particles of reduced dimensions. Finally, the predicted occurrence of icosahedral precursors to melting of clusters may result in relatively enhanced melting temperatures for cluster sizes corresponding to icosahedral-packing magic numbers (e.g., 55, 147, 309, ...); indeed, an indication of such a trend has been most recently reported for sodium clusters [20].

This research was supported by the U.S. Department of Energy. Calculations were performed at the GIT Center for Computational Materials Science.

- [1] W. Thomson, *Philos. Mag.* **42**, 448 (1871).
- [2] P. Pawlow, *Z. Phys. Chem.* **65**, 545 (1909).
- [3] Ph. Buffat and J.P. Borel, *Phys. Rev. A* **13**, 2287 (1976).
- [4] S. Iijima, in *Microclusters*, edited by S. Sugano *et al.* (Springer, Berlin, 1987), p. 186.
- [5] T. Castro *et al.*, *Surf. Sci.* **234**, 43 (1990).
- [6] F. Ercolessi, W. Andreoni, and E. Tosatti, *Phys. Rev. Lett.* **66**, 911 (1991).
- [7] (a) H.-P. Cheng and R.S. Berry, *Phys. Rev. A* **45**, 7969 (1992); (b) R.S. Berry, in *Clusters of Atoms and Molecules*, edited by H. Haberland (Springer, Berlin, 1994), pp. 187–204.
- [8] S. Valkealahti and M. Manninen, *Comput. Mater. Sci.* **1**, 123 (1993).
- [9] T.P. Martin *et al.*, *J. Chem. Phys.* **100**, 2322 (1994).
- [10] C.L. Cleveland, U. Landman, and W.D. Luedtke, *J. Phys. Chem.* **98**, 6272 (1994).
- [11] O.H. Nielsen *et al.*, *Europhys. Lett.* **26**, 51 (1994).
- [12] L.D. Marks, *Rep. Prog. Phys.* **57**, 603 (1994).
- [13] L.J. Lewis, P. Jensen, and J.-L. Barrat, *Phys. Rev. B* **56**, 2248 (1997).
- [14] M. Schmidt *et al.*, *Phys. Rev. Lett.* **79**, 99 (1997).
- [15] J.F. Van der Veen *et al.*, in *Kinetics of Ordering at Surfaces*, edited by M.G. Lagally (Plenum, New York, 1990), p. 343; see also Ref. [10].
- [16] (a) C.L. Cleveland *et al.*, *Phys. Rev. Lett.* **79**, 1873 (1997); (b) R.L. Whetten *et al.*, *Adv. Mater.* **5**, 428 (1996); (c) C.L. Cleveland *et al.*, *Z. Phys. D* **40**, 503 (1997).
- [17] D. Faken and H. Jonsson, *Comput. Mater. Sci.* **2**, 279 (1994).
- [18] A. Guinier, *X-Ray Diffraction* (Freeman, San Francisco, 1963).
- [19] T.P. Martin, *Phys. Rep.* **95**, 167 (1983).
- [20] M. Schmidt *et al.*, *Nature (London)* **393**, 238 (1998); H. Haberland (private communication).